Oil Extraction From Spent Coffee Grounds As Green Corrosion Inhibitor for Copper in 3 wt% NaCl Solution

Ghada ROUIN , Makki ABDELMOULEH , Abdulrahman MALLAH , Mohamed MASMOUDI *

Posted Date: 8 June 2023

doi: 10.20944/preprints202306.0568.v1

Keywords: Corrosion; copper; spent coffee grounds; voltammetry around OCP; EIS

 doi:10.20944/preprints202306.0568.v1

Article

Oil Extraction from Spent Coffee Grounds as Green Corrosion Inhibitor for Copper in 3 wt% NaCl Solution

Ghada ROUIN [1], Makki ABDELMOULEH [2], Abdulrahman Mallah [3] and Mohamed MASMOUDI [1,4,*]

[1] Laboratory of electrochemistry and environment (LEE), National Engineering School, BPW, 3038 Sfax, University of Sfax, Tunisia
[2] Laboratory of Materials Sciences and Environment (LMSE), Faculty of Sciences of Sfax.
[3] Department of Chemistry, College of Science, Qassim University, P.O. Box 6644, Buraydah Almolaydah, Buraydah 51452, Saudi Arabia
[4] Preparatory Institute for Engineering Studies of Sfax, BP 805, 3018,University of Sfax.
* Correspondence: med_mmasmoudi@yahoo.fr.

Abstract: This work aims to follow the corrosion behavior of copper in 3 wt% NaCl solution in the presence of a bio-oily extract. Spent coffee grounds (SCG), a highly recyclable and usable biomass - often thrown away and becoming a serious threat to the environment - , has a fraction of oils (12%) that we have opted to use as a corrosion inhibitor for copper. The extraction was carried out using n-hexane as the solvent for the decoction. The oily fraction was analyzed by Fourier transform infrared spectroscopy (FTIR) and thermogravimetric analysis (TGA). Potentiodynamic polarization measurements have revealed SCG extract acts as a cathode-type inhibitor for copper in saline media, mainly preventing the diffusion of oxygen molecules toward the substrate. As the extract concentration increased, the inhibition efficiency has improved as well, reaching 95.78 % with 0.6 g/L of SCG extract. The obtained results by electrochemical impedance spectroscopy (EIS) are in accordance with the order of inhibitory efficiency obtained by potentiodynamic polarization. We have found that the SCG extract adsorption process on copper surface is spontaneous and complies with Langmuir isotherm.

Keywords: corrosion; copper; spent coffee grounds; voltammetry around OCP; EIS

1. Introduction

Copper, classified as a noble metal, is often used because of its corrosion resistant properties. It's a material that is extensively used in a variety of industries, including electronics and the production of integrated circuits, as it has excellent electrical and thermal conductivities [1]. However, copper can be easily corroded in the presence of aggressive ions such as chloride, which greatly limits its use [2]. Generally, corrosion is an important economic, environmental and safety issue. Each year, damages resulting from corrosion amount to hundreds of billions of dollars [3]. Corrosion not only wastes raw materials and energy but also causes serious accidents and - in some case - contributes to the environment's pollution.

Corrosion problems are increasingly being taken into account. Studying copper's corrosion in aqueous media is primarily intended to serve the industrial action of corrosion control [4–6]. Most of the inhibitors are organic elements with atoms of sulfur, phosphorous, nitrogen and oxygen. Their adsorption on the metal surface is frequently responsible for the inhibitory action [7]. Current research is increasingly moving towards the use of green inhibitors. Their non-toxic and biodegradable nature has favored their use as ecological inhibitors. An environmentally friendly and potentially renewable resource alternative for chemical-based compounds is wasted food. Currently,

 doi:10.20944/preprints202306.0568.v1

sustainable corrosion protection methods that adhere to "green chemistry" principles are being developed [8–13].

Coffee is the second most important commercial product that creates a large amount of spent coffee grounds (SCG) every year [14,15]. According to the literature, used coffee grounds are a great source of value-added energy as well as non-energy-related products due to their substantial amounts of fatty acid, cellulose, esters, lignin and hemicelluloses … [16–18]. Some studies have investigated the effect of SCG extract on corrosion inhibition in different metals and environments [19–23]. As far as we know, one of them used copper as substrate and NaCl as electrolyte. Velazquez-Torres et al [22] used the fatty amide derived from coffee oil as an inhibitor for corrosion, prepared through the direct aminolysis of oil extract and hydroxyethyl ethylenediamine. They found that the N-[2-[(2-hydroxyethyl) amino] ethyl]-amide extracted from coffee residue is a mixed inhibitor for the copper in 3.5 wt% NaCl solution.

The main objective of the current research focuses on the examination of corrosion inhibition of copper in saline solution by the SCG oil extract under different inhibitor concentrations. Thus, the electrochemical techniques including potentiodynamic polarization on a wide potential range, voltammetry around OCP and electrochemical impedance spectroscopy (EIS) were used.

2. Experimental

2.1. Inhibitor preparation

We dry the SCG in an oven at 60 °C for 24 hours. After drying, we have investigated an extraction procedure: 3-hour decoction procedure in 100 mL n-hexane at 78°C. The extract was filtered, and the hexane extract was evaporated by a rotavaporator with a vacuum as mentioned in **Figure 1** (step 1). For the preparation of the inhibitor solution, a mass of oil was dissolved in tween 80 (m, 1/2 m), obtaining concentrations of 0.2, 0.4 and 0.6 g/L. The corrosion solution was then prepared using the SCG extract concentrations as the inhibitor in a 3 wt% NaCl solution. The influence of SCG extract concentration and time immersion of inhibitor in chloride solution was studied at room temperature (25 ± 2 °C) (**Figure 1**, step 2).

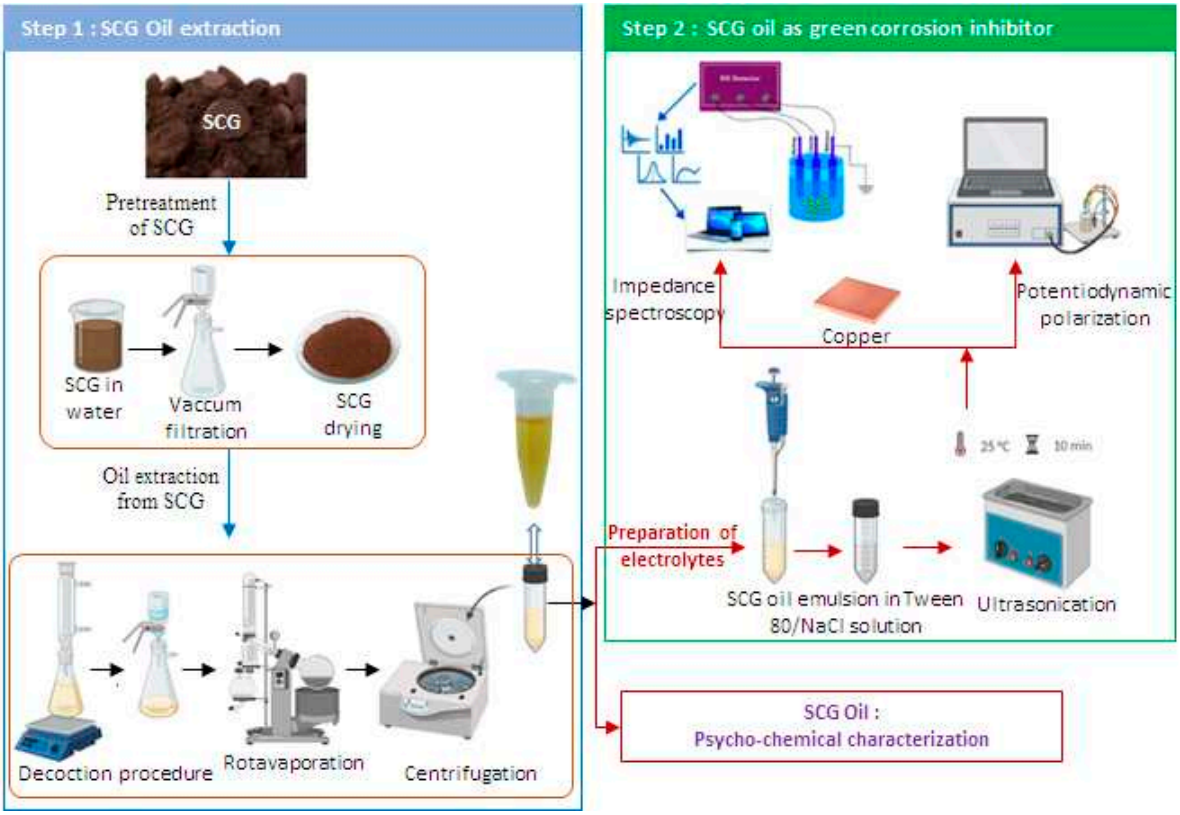

Figure 1. The two-step process of SCG oil extraction and its use as an inhibitor for copper corrosion.

 doi:10.20944/preprints202306.0568.v1

2.2. Characterization of the spent coffee grounds extract

We have obtained the FTIR (ATR) spectra of samples by a Perkin Elmer spectrometer. We have scanned each sample at a wave number range of 400–4000 cm^{-1} with a resolution of 2 cm^{-1} for each spectrum. The thermogravimetric (TGA) curves of the SCG samples were obtained using TA Instruments TGA Q500. All the samples were investigated from 30 to 800 °C at a heating rate of 10 °C/min under air atmosphere.

2.3. Electrochemical measurements

We have used an electronic potentiostat galvanostat radiometer PST050 controlled to take the electrochemical measurements through the Volta Lab software while the electrochemical analyses were conducted under computer control.

We have carried out the electrochemical techniques (potentiodynamic polarization and electrochemical impedance spectroscopy) in a classical three-electrode cell. Pure copper (99.99 %), platinum foil and saturated calomel electrode (SCE) were used as working, counter and reference electrodes, respectively. The epoxy resin masked the copper electrodes, leaving 100 mm^2 as the working surface.

Before each test, we polished the exposed surface of copper with SiC paper (from grade 240 to grade 1200), washed it with distilled water, degreased it with acetone and finally dried in warm air.

We plotted potentiodynamic polarization curves from - 400 to 400 mV/SCE at a polarization rate 0.5 mV/ second. Prior to all the experiments, we stabilized the potential of the working electrodes for 90 minutes of immersion at the open circuit potential (OCP) of the electrodes.

This immersion period was chosen after testing five-immersion times (30, 60, 90, 120 and 150 minutes).

We made the voltammetry around OCP measurements at 90-minute immersion of the working electrode at room temperature under OCP conditions. The potential was swept from OCP –60 mV to OCP +60 mV at a scan rate dE/dt = 0.5 mV/second.

The polarization curves, obtained on a limited range of potential around OCP, created only a slight perturbation of the metal surface. The experimental curves fit indicate that the anodic and cathodic reactions comply with Tafel's law. The experimental function which was used to mathematically model the potentiodynamic polarization curve (ΔE = ± 60 mV) is given by Equation (1) [24,25]:

$$j = j_a + j_c = j_{corr}\left[e^{\beta_a(E-E_{corr})} - e^{\beta_c(E-E_{corr})}\right] \quad (1)$$

Where β_a and β_c are the anodic and the cathodic Tafel coefficient, in mV/dec, respectively.

The electrochemical impedance spectroscopy (EIS) measurements were taken after stabilization for a 90-minute immersion at OCP by a sinusoidal signal with an amplitude of 10 mV over a frequency ranging from 100 kHz to 0.1 Hz under the excitation of a 10 mV AC perturbation signal. The impedance spectra fitting were achieved via electrical equivalent circuits. They were fitted by means of a "Randomize + Simplex" fitting mode with the EC-Lab V10.32 software and the maximum number of iterations set at 10000.

3. Results and discussion

3.1. FT-IR spectral analysis

The virgin SCG's FTIR spectrum - pretreated SCG, de-oiled SCG and SCG oil - are presented in **Figure 2**.The lists of functional groups identified were shown in **Table 1**. Examination of FTIR spectrums of all SCG-based samples has revealed a wide vibration at around 3320 cm^{-1} which was attributed to OH stretching vibrations, demonstrating the presence of phenols or alcohols stemmed from lignin content of the biomass feedstock [26]. The absorption peaks between 2858 cm^{-1} and 2924 cm^{-1} were attributed to asymmetric and symmetric stretching vibration of C-H bonds of aliphatic CH_2 group [27]. The FTIR spectrum exhibiting all characteristic peaks of lipid compounds indicated the presence of the oil in the SCG [27]:

 doi:10.20944/preprints202306.0568.v1

(i) We can notice the vibration of the ester carbonyl group C=O taking place between 1740 cm^{-1} and 1744 cm^{-1} characteristic of carbonyls of lipids, esters and carboxylic acids [28]

(ii) The region about 1639 cm^{-1} corresponds to C=C.

The vibration bands taking place between 1000 and 1100 cm^{-1} corresponds to the C-O and C-C-O bonds attributed to the structure of cellulose, hemicellulose and lignin [29]. The wavenumber range of 1400-900 cm^{-1} was marked by vibrations of several bond types, including C-H, C-O and C-N resulted from absorption band of carbohydrates and several special compounds in the coffee beans (chlorogenic acids) [30,31]. The most relevant changes between the spectra of the virgin SCG and pretreated SCG observed in the OH stretching (3315 cm^{-1}) and the carbonyl stretching vibrations (1744 cm^{-1}) regions confirm the removal of water-soluble compounds by the pretreatment step. The absence of the most characteristic high levels for the lipid compounds in the spectroscopy of the de-oiled sample indicated that coffee oil might be completely extracted in hexane solvent by decoction method [27].

Indeed, the FTIR spectrum of the extracted oil sample -using the process adopted in our work- from the coffee grounds powder shows the presence of all the characteristic bands of the groups of the oily compounds. Thereby, the FTIR spectra of SCG oil from decoction extraction shows the wavenumber at 3009 cm^{-1} assigned to C-H stretching vibration of *cis* double bond, which indicates the presence of unsaturated fatty acids [27,32]. The absorption peaks 2921 cm^{-1} and 2853 cm^{-1} were typically attributed to C-H stretching vibration which was assigned to alkyl groups, indicating the presence of hydrocarbons in SCG oil [26]. The triglyceride is represented by peaks at 1746 cm^{-1} and 1161 cm^{-1} which corresponds to carbonyl group (-C=O stretch) and esters groups (-C-O stretch), respectively [33]. The C-H bending is represented by peaks at 1376-1463 cm^{-1} corresponding to alkane groups. The absorption between 1161 cm^{-1} and 1099 cm^{-1} resulted from C-O stretching vibration which corresponds to esters groups present in the SCG oil. Furthermore, the peak at 721 cm^{-1} indicates the existence of (=C-H) bending and *cis*-disbstituted alkenes [34].

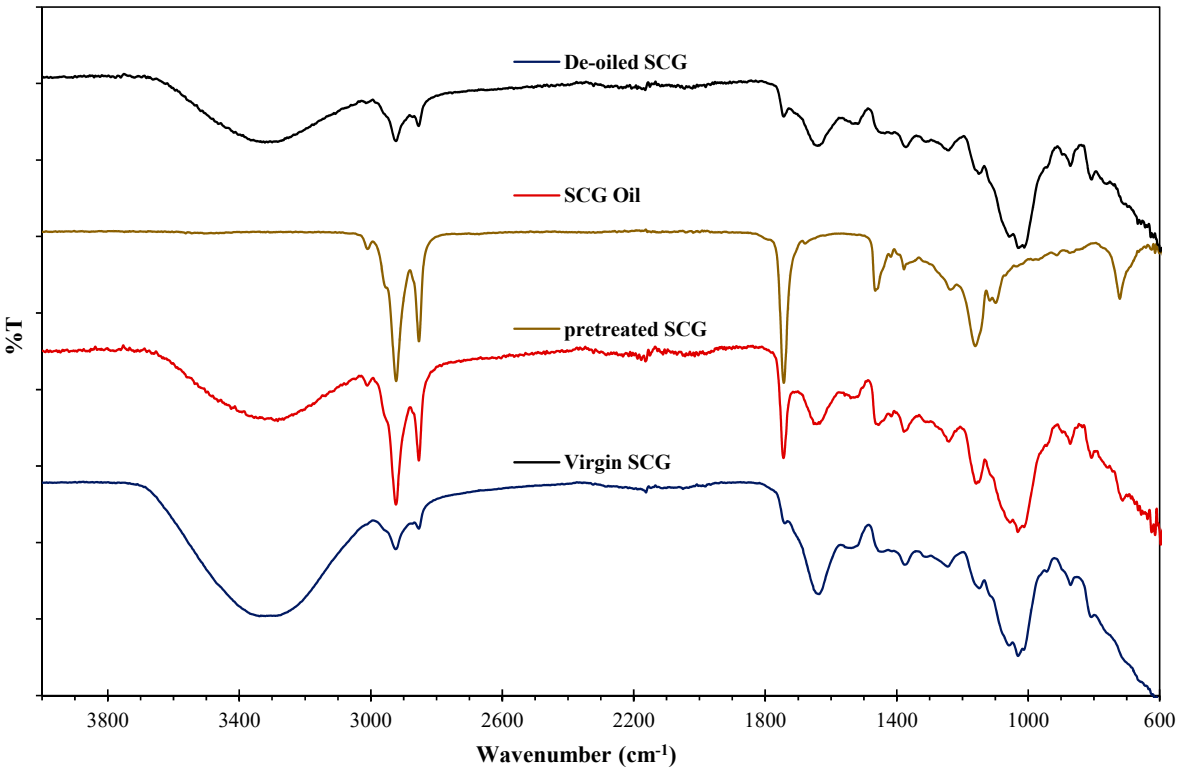

Figure 2. FTIR spectrums of SCG samples and SCG oil.

 doi:10.20944/preprints202306.0568.v1

Table 1. Analytical evaluation of infrared spectra of SCG samples and SCG Oil.

Wavenumbers (cm^{-1}).		**Attributions**
SCG samples	*SCG Oil*	
3312	---	O–H stretching vibration
---	3009	C-H stretching symmetric vibration of the *cis* double bonds [35]
2924	2921	Asymmetric and symmetric stretching vibration of C–H bonds of aliphatic
2858	2853	CH_3[32,35]
1740	1746	Stretching vibration of ester carbonyl functional groups (C=O)
1463	1463	Bending vibration of C-H of CH_2 and CH_3 aliphatic group
1640		C=C stretching vibration cis-olefins [35]
1369	1376	Bending symmetric vibration of C-H bonds of CH_2 groups [35]
1100	1161	Stretching vibration of C-O-C ester groups [36]
1400-900	1400-900	Stretching vibration of (C-O), (C-H), (C-N) [27,31,37]
721	721	=C-H Aliphatic CH_2 rocking vibration and *cis* substituted olefin out-of-plane vibration overlapping [32,38]

3.2. Thermogravimetric analysis:

The results of TGA analyses are collected in Figure 3. The TGA curves of all SCG samples occurred mainly in three decomposition stages. The first degradation stages lower than 130 °C were attributed to the removal of adsorbed water on SCG powders. In this temperature ranges, the mass losses occur at levels for 47 % for virgin SCG, 5 % for pretreated SCG, and 9 % for de-oiled SCG. The high loss value on virgin SCG is essentially due to the residual water molecules' presence in the powder structure of SCG recovered as waste. The relatively high mass loss value for de-oiled SCG compared to that of pretreated SCG may be related to the high accessibility of de-oiled SCG powders after extraction of the oily phase, which can create a barrier to the adsorption of water molecules. The greatest transformation and mass losses take place during the second stage at roughly 250 ºC. At this stage, the depolymerization as well as decomposition of polysaccharides (cellulose, hemicellulose, lignin) [39] and some oils present in the sample happens [39].The third stage, occurring at temperatures above 550 °C and at a very low rate of mass loss, reveals the carbonaceous solid's formation [28]. The residual mass obtained above 550°C is much clearer in the virgin SCG sample, which is linked to the presence of solid impurities or inorganic compounds in the SCG waste.

The TGA curve of SCG oil in air atmosphere (**Figure 3**) has revealed that mass loss did not take place at temperature below 150 °C, indicating that there is no solvent in the extracted oil. Thermal decomposition of the SCG oil completely happens in two stages between 150 and 650 °C [27,40].

Preprints.org (www.preprints.org) | NOT PEER-REVIEWED | Posted: 8 June 2023 doi:10.20944/preprints202306.0568.v1

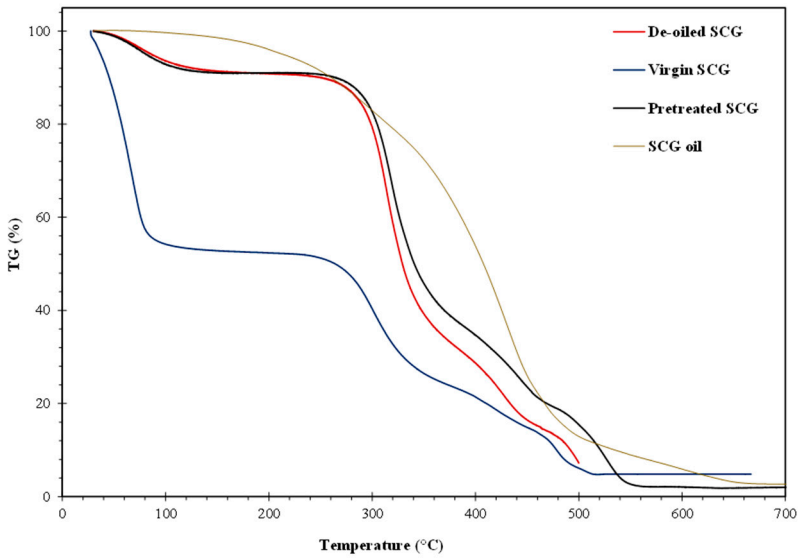

Figure 3. Thermogravimetric curves of virgin SCG, pretreated SCG, de-oiled SCG and SCG oil.

3.3. Electrochemical studies

3.3.1. Potentiodynamic polarization between - 0.4 and + 0.4 V/SCE

Figure 4 reveals the potentiodynamic polarization curves of copper after a 90-minute immersion in 3 wt% NaCl solution without (blank) and with SCG oil extracts at 25°C.

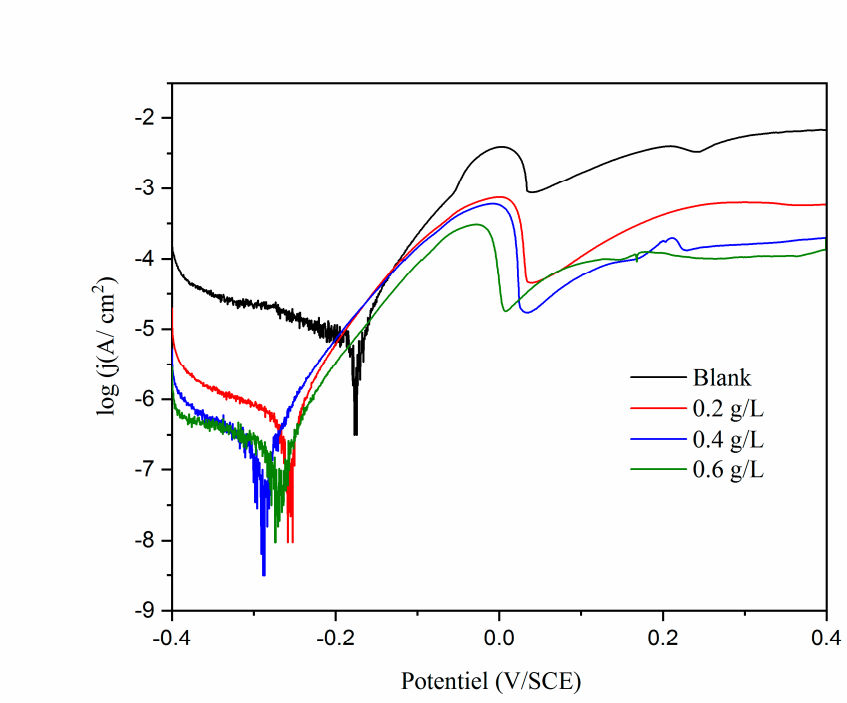

Figure 4. Polarization curves of copper exposed to 3 wt% NaCl solutions devoid of (blank) and containing different concentrations of SCG extract at RT (~25 °C).

We can confirm from this figure that the cathodic branch of the copper in the blank chloride solution can be divided into three regions: region I corresponds to the weak polarization region near OCP; next, region II corresponds to nearly flat current density, associated with the reduction of

 doi:10.20944/preprints202306.0568.v1

dissolved oxygen (Equation (2)); and region III, almost below -380 mV, is the result of the hydrogen evolution reaction mentioned in Equation (3) [24,41]

$$O_2 + 2H_2O + 4e^- \rightarrow 4OH^- \quad (2)$$

$$2H_2O + 2e^- \rightarrow H_2 + 2OH^- \quad (3)$$

$$O_2 + 2H_2O + 4e^- \rightarrow 4OH^- \quad (2)$$

$$2H_2O + 2e^- \rightarrow H_2 + 2OH^- \quad (3)$$

Both metal electro-dissolutions and metal soluble diffusion in the blank solution control the anodic reaction. As it was stated in our previous research, the dissolution mechanism can be represented by the following reactions [42]:

$$Cu \rightarrow Cu^+ + e^- \quad (4)$$

$$Cu^+ + Cl^- \rightarrow CuCl_{(film)} \quad (5)$$

$$CuCl + Cl^- \rightarrow CuCl^-_{2(surface)} \quad (6)$$

Figure 4 also shows that the presence of SCG extract shifted the cathodic branch of the polarization curves towards more negative potentials and toward a lower current density. Thus, confirming that this oil extract has a stronger impact on oxygen cathodic reduction than on copper oxidation reaction. The E_{corr} values measured for the blank, 0.2g/L; 0.4g/L and 0.6g/L solutions are respectively equal to -176, -272, -287 and -274 mV/SCE. Consequently, the E_{corr} shift reaches 111 mV/SCE for 0.4 g/L, a value which is sufficiently high to classify the SCG extract as a cathodic inhibitor [5,24].

3.3.2. Voltammetry around OCP (ΔE=± 60 mV)

To further explain the SCG oil extract corrosion resistance performance, potentiodynamic polarization curves were obtained after a 90-minute immersion in 3 wt% NaCl solution with the addition of oil extract at different concentrations on a limited potential range (ΔE= ±60 mV). These curves were computer fitted using the EC-Lab program V10.32 (Bio-Logic) as described in section 2.3 to first determine the corrosion current density (J_{corr}), the Tafel coefficients (β_a and β_c) and the corrosion rate (CR) and to later calculate the polarization resistance (R_p) and the inhibition efficiency (η %) according to Equations (7,8) and (9), respectively.

$$R_p = \frac{B}{J_{corr}} \quad (7)$$

Here B is a constant that is calculated by using Stern-Geary Equation [43],

$$B = \frac{\beta_c \, \beta_a}{2.303 \, (\beta_c + \beta_a)} \quad (8)$$

$$\eta \, (\%) = \frac{CR^0 - CR}{CR^0} \times 100 \quad (9)$$

Where CR^0 and CR are the corrosion rate in the absence and presence of inhibitor, respectively. In **Table 2**, all of these electrochemical parameters were reported.

Table 2. Electrochemical kinetic parameters and inhibition efficiency obtained from potentiodynamic polarization curves (ΔE= ±60 mV) after a 90-minute immersion in 3 wt% NaCl solution at RT (~ 25C°).

E	E_{corr} (mV/SCE)	J_{corr} µA cm^{-2}	βa (mV/dec)	-βc (mV/dec)	CR mm year^{-1}	Rp (kΩ.cm^2)	η (%)
Blank	-176 ±2	5.41 ± 1.2	40 ± 13	120 ± 5	0.063 ± 1.1	2.40 ±1.3	–
0.2g/L	-272 ±4	0.745 ± 0.3	45.4 ± 2	62.8 ± 6	0.00868 ± 0.3	15.35 ± 2	86.22 ±5
0.4g/L	-287 ±3	0.305 ± 0.3	59.6 ± 7	60.7±14	0.00355 ± 0.3	42.81±1.4	94.36 ±4
0.6g/L	-274 ±4	0.228 ± 0.2	46.8 ± 2	95.9 ± 2	0.00265 ± 0.2	59.89 ± 2.8	95.78 ±3

 doi:10.20944/preprints202306.0568.v1

Figure 5 illustrates an example of comparison between the experimental polarization curve and Tafel curve simulated with EC-Lab software for copper with addition of SCG oil for 0.4g/L in saline solution.

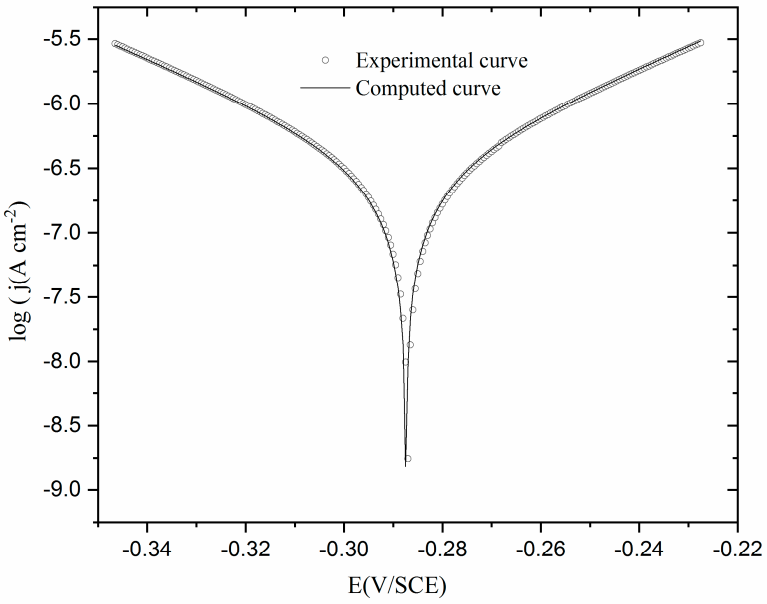

Figure 5. Experimental polarization curve around OCP exposed to 3 wt % NaCl solutions containing 0.4 g/L of SCG oil at RT (~25 °C) and computed curve.

In the experimental conditions that we used, the cathodic branch reveals the reactions of oxygen reduction and the anodic branch corresponding to the copper dissolution [44]. It can be noted that in the presence of SCG oil extract, the anodic Tafel slopes (β_a) have roughly constant with an average value of 50 ±7 mV/dec. This finding indicates that the presence of SCG oil has no major effect on the copper dissolution. The cathodic Tafel coefficient (β_c) was determined at 120 mV/dec in the blank solution. These values decrease after adding inhibitor to reach 60.7 ± 14 mV/dec for 0.4 g/L SCG oil concentration, which may be linked to the fact that the inhibitor mainly impacts the cathodic reaction. As it was shown in **Table 2**, the values of J_{corr} drop with the inhibitor concentration' rise, indicating a remarkable decrease in the CR which reaches a minimum value of 0.0026 mm/year and a significant increase in the polarization resistance, especially with 0.6 g/L (Rp = 59.89 ± 2.8 kΩ.cm²). In addition, the inhibition efficiency (η) reached 95.78 % in the 0.6 g/L concentration of SCG oil extract. This confirms that SCG oil shows a good inhibition effect on copper in chloride media. Thus, the high concentration could boost protection ability against copper corrosion.

3.3.3. Electrochemical impedances spectroscopy (EIS)

Figure 5 reveals the Nyquist diagrams obtained after a 90-minute immersion in 3 wt% NaCl solution without and with various concentration of inhibitor at 25°C. The Nyquist diagram obtained without inhibitor (blank) shows a capacitive semicircle at high frequencies with a straight line inclined characteristic of a Warburg-type diffusion process at low frequencies. This semicircle shows the combination of charge transfer resistance as well as double layer capacitance. It should be noted that this capacitive loop is not completely perfect; this can be attributed to the roughness and inhomogeneity of the electrode surface [24,45,46]. The straight line could be attributed to the anodic diffusion of soluble copper species of $CuCl_2^-$ from the electrode to the chloride solution, and to the cathodic oxygen's diffusion [25].

 doi:10.20944/preprints202306.0568.v1

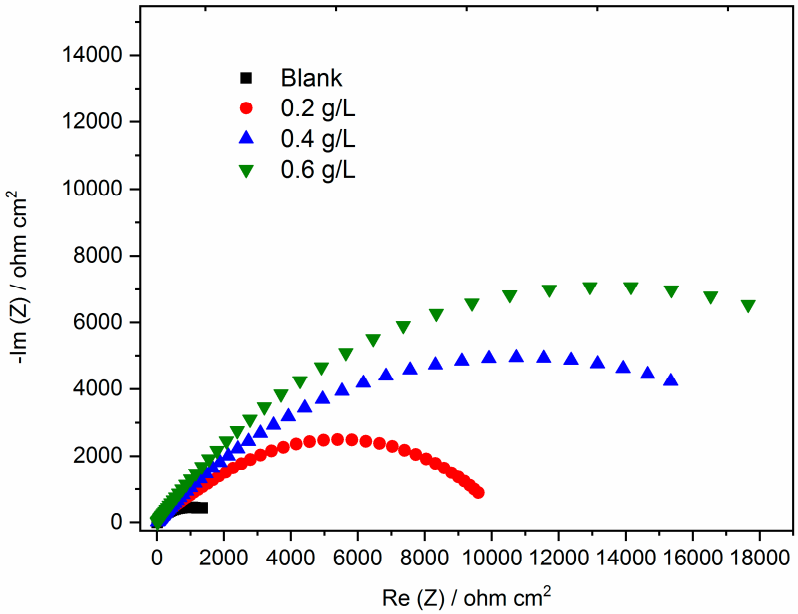

Figure 5. Nyquist plots for copper exposed to 3 wt% NaCl solutions devoid of (blank) and containing different concentrations of SCG oil at RT (~25 °C).

The appearance of copper's Nyquist curves in a 3 wt% NaCl solution in the presence of different concentrations of the SCG oil extract are fairly distinct from that of the copper in the absence of the SCG oil. This means that the change in the corrosion mechanism occurs following the inhibitor's addition. The size of the capacitive loops seems to grow with the increase in extract concentration. In fact, the Nyquist loop's diameter for a concentration of 0.6 g/L of SCG oil extract was significantly larger than that for the other electrode. This might be because the extract's protective layer adheres to copper surface and compacts when the concentration increases [47]. Hence, it forms a stable layer on the metal surface functioning as an efficient barrier that prevents corrosion.

The logarithm of impedance amplitude (log |Z|) as a function of the logarithm of frequency (log freq) is represented in **Figure 6a**. At low frequencies, the amplitude of the bare copper's impedance |Z| is lower (around $10^3\ \Omega\ cm^2$), indicating that the material easily corrodes because the CR and the value of |Z| are inversely related [48]. For the same frequency range, the |Z| value of copper was significantly higher after the inhibitor's addition, particularly at 0.6 g/L (around $10^4\ \Omega\ cm^2$). Finally, the log |Z| becomes practically constant when the frequency is low. We can also observe an increase in the resistive response of the copper electrode [49].

Preprints.org (www.preprints.org) | NOT PEER-REVIEWED | Posted: 8 June 2023 doi:10.20944/preprints202306.0568.v1

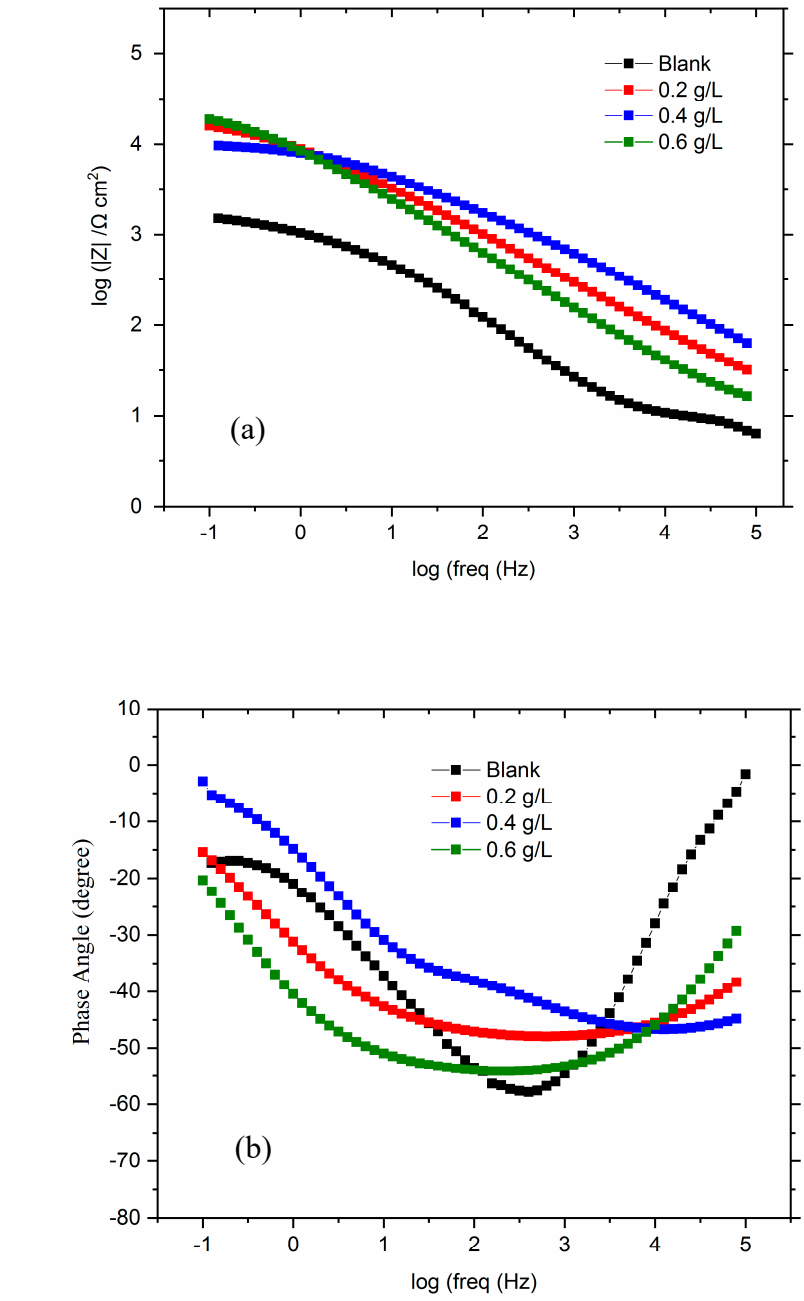

Figure 6. Bode plots (a) and phase angle (b) versus frequency for SCG oil for copper exposed to 3 wt % NaCl solutions at RT (~25 °C).

Figure 6b displays the phase angle plots of copper without and with various concentration of SCG oil extract after a 90-minute immersion in 3 wt% NaCl solutions. The argument of the complex impedance Z (phase shift between the current and the potential), Arg (Z) is plotted as the logarithm of frequency's function. The phase angle plots obtained for the copper in blank saline solution reveals two-time constants: the first in the high frequency region, related to the relaxation process of the double layer capacitance and the second in the low frequency region, corresponding to the Warburg diffusion (corrosion process) [41].

 doi:10.20944/preprints202306.0568.v1

Two-time constants can be seen on the curves after adding the working oil. One was in the higher frequency caused by the presence of the inhibitor while the other was shown at medium frequencies related to the double layer capacity.

In harmony with the earlier EIS findings' description, the impedance data's analysis was carried out with two equivalent circuits presented in **Figure7**.

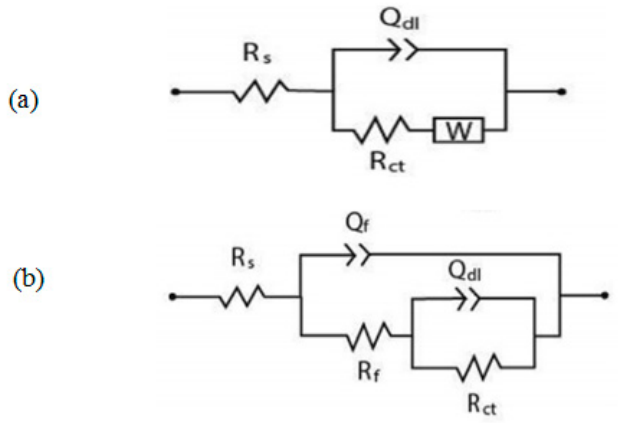

Figure 7. Equivalent circuits used to fit the EIS experimental data.

We describe the behavior of copper or copper alloys in chloride-containing solutions by means of these models in the literature, either without or with the adsorption of inhibitors [50,51]. **Figure 7a** proves suitable for the experimental impedance data of copper in the blank solution. In this model, R_s is the solution resistance, R_{ct} is the charge transfer resistance, Q_{dl} corresponds to the capacitance of the double layer as well as W is the Warburg impedance linked to the diffusion processes in the low frequency region [24]. In contrast, it was fair to use the equivalent circuit $R_s(Q_f(R_f(Q_{dl}R_{ct})))$ **(Figure 7b)** to analyze the copper's EIS data in solutions containing SCG oil. This equivalent circuit consists of passive film resistance (R_f) and passive film capacitance (Q_f).

The "dispersion effect" at the solid/liquid interface was clearly present because the impedance loops' centers - located below the real axis (see **Figure 5**) - are not perfect semicircles. The solid electrode surface's inhomogeneity and roughness are behind this phenomenon [52]. It is, therefore, required to replace the pure capacitor with a constant phase element CPE (Q) when fitting the EIS data in order to obtain a fit that is more accurate. We can calculate the impedance of CPE as follows to Equation (10) [53]:

$$Z_{\mathrm{CPE}} = {}^{1}/_{Q_0(j\omega)^{\mathrm{n}}} \quad (10)$$

where Q_0 is the magnitude of CPE, j is the imaginary root, ω is the angular frequency, and n value is attributed to the electrode's inhomogeneous nature due to the surface roughness, porous layer formation, inhibitor adsorption, etc[54].

The electrochemical parameters obtained after EIS data's computer fitting through electric circuits shown in **Figure 7** are listed in **Table 3**.

Inhibition efficiency (η) can be calculated by the polarisation resistance as it was shown in Equation (11) [53]:

$$\eta = \frac{R_{\mathrm{p}} - R_{\mathrm{p}}^{0}}{R_{\mathrm{p}}} \times 100 \quad (11)$$

R^{0}_{p} and R_{p} are the polarization resistance of copper in 3 wt % NaCl solutions devoid of and containing SCG oil extract, respectively.

The value of R_{p} can be applied as an anti-corrosion ability's indicator calculated according to the following of Equation (12) [55]:

$$R_{\mathrm{p}} = R_{\mathrm{ct}} + R_{\mathrm{f}} \quad (12)$$

The first remark derived from the data in **Table 3** is that the parameters obtained without inhibitor (blank) correlate with previously published research [24,48,55]. Furthermore, compared to

 doi:10.20944/preprints202306.0568.v1

the parameters we got after adding the working oil, we can see that the lowest value of R_{ct} (1466 Ω cm²) was obtained for the blank sample, showing the inhibition effect of SCG oil on copper electrode. **Table 3** also shows that R_{ct} values increased from 1466 to 17980 Ω cm² with the rise in SCG oil concentrations. Increased R_{ct} values with SCG oil concentration are based on the rise in inhibitor surface coverage, resulting in an increase in inhibitor efficiency [56]. In addition, the R_f value rose from 3698 Ω cm² in 0.2 g/L SCG oil concentration to 8932 Ω cm² in 0.6 g/L oil concentration. Thus, the R_p value concerning 0.6 g/L of SCG oil equals 26822 Ω cm² which is 18-fold higher than that of the blank solution. As it is noticed in **Table 3**, the inhibition efficiency (η) of SCG increases from 85.93% to 94.55%, when the oil's concentration rises from 0.2 g/L to 0.6 g/L%. These values are in accordance with η values derived from the potentiodynamic polarization curves recorded around OCP (**Table 2**). Hence, it has been demonstrated that the inhibitor forms a stable layer on the copper surface that acts as an efficient barrier that prevents corrosion.

Table 3. Electrochemical parameters and inhibition efficiency obtained from EIS study of copper electrode after 90 min of immersion in 3 wt % NaCl solutions without (blank) and with various concentrations of SCG extract at 25°C.

	Blank	0.2 g/L	0.4 g/L	0.6 g/L
$Rs\ (\Omega\ cm^2)$	6.915	7.03	8.4	9.02
$R_{ct}\ (\Omega\ cm^2)$	1466	6725	13 985	17 980
$Q_{dl}\ \times 10^{-6} (F\ cm^{-2}\ s^n_{dl})$	145	7.42	6.836	7.2
n_{dl}	0.687	0.67	0.4	0.53
$R_f\ (\Omega\ cm^2)$	–	3698	7821	8932
$Q_f\ \times 10^{-6}\ (F\ cm^{-2}\ s^n_f)$	–	10.88	25.03	26.76
$Rp\ (\Omega\ cm^2)$	1466	10 423	21 806	26 822
n_f	–	0.559	0.557	0.63
$W\ (\Omega^{-1}\ cm^{-2}\ s^{0.5})$	140.2	–	–	–
$\eta\ (\%)$	–	85.93	93.27	94.55

3.3.4. Adsorption isotherms modeling

It is generally known that organic molecules inhibited corrosion by adsorption at the metal/solution interface. The adsorption isotherms can be used to provide fundamental details regarding the interaction between inhibitors and a metal surface. The adsorption of an organic adsorbate at the metal-solution interface can occur because of the substitution in the aqueous solution ($Org_{(sol)}$) and water molecules previously adsorbed on the metallic surface ($H_2O_{(ads)}$) according to the following Equation (13) [57]:

$$Org_{(sol)} + xH_2O_{(ads)} \rightarrow Org_{(ads)} + xH_2O_{(sol)} \quad (13)$$

Where $Org_{(sol)}$ and $Org_{(ads)}$ are the organic compounds present in the aqueous solution and the organic molecules adsorbed onto the metal surface, x is the ratio indicating the number of water molecules that are substituted by one organic adsorbate molecule [58].

In order to evaluate the adsorption process of SCG oil extract on the copper surface, various isotherms were used namely Langmuir, Frumkin, Temkin, Freundlich and Flory Huggins isotherms according to the following Equations (14-18) [25]:

Langmuir
$$\frac{C}{\theta} = \frac{1}{K_{ads}} + C \quad (14)$$

Frumkin
$$\ln\left[\frac{\theta}{(1-\theta)C}\right] = 2a\theta + \ln K_{ads} \quad (15)$$

Temkin
$$\ln C = a\,\theta - \ln K_{ads} \quad (16)$$

Freundlich
$$\log\theta = n \log C + \log K_{ads} \quad (17)$$

Flory–Huggins
$$\log\frac{\theta}{C} = \log(xK_{ads}) + x\log(1-\theta) \quad (18)$$

 doi:10.20944/preprints202306.0568.v1

Where θ is the surface coverage determined through the relation θ = η/100, and from the impedance data, C is the concentration of SCG oil, K_{ads} is the adsorption-desorption equilibrium constant, a is the parameter of later interaction between the adsorbate species which is a strong indicator of the non-homogeneity of the surface, n is the Freundlich adsorption isotherm parameter [25,59].

To select the isotherm that best fits the experimental data, various correlation coefficients (R^2) was determined for several classical adsorption isotherms. R^2 determined from the Langmuir adsorption isotherm gives the best fit (R^2= 0.999). This behavior suggests that the species present in the SCG oil extract were adsorbed onto the copper surface according to a Langmuir adsorption isotherm. It involves the formation of a protective monolayer on the metal surface with a fixed number of actives sites [60].

A straight line is acquired by plotting of C/θ versus C as shown in **Figure 8.** The intercept of the straight line obtained in the Langmuir adsorption isotherm was used to calculate K_{ads} for the SCG oil extract. The high value of K_{ads} (32.89 g^{-1}.L) exhibits the high adsorption ability of the working oil on the metal surface [61].

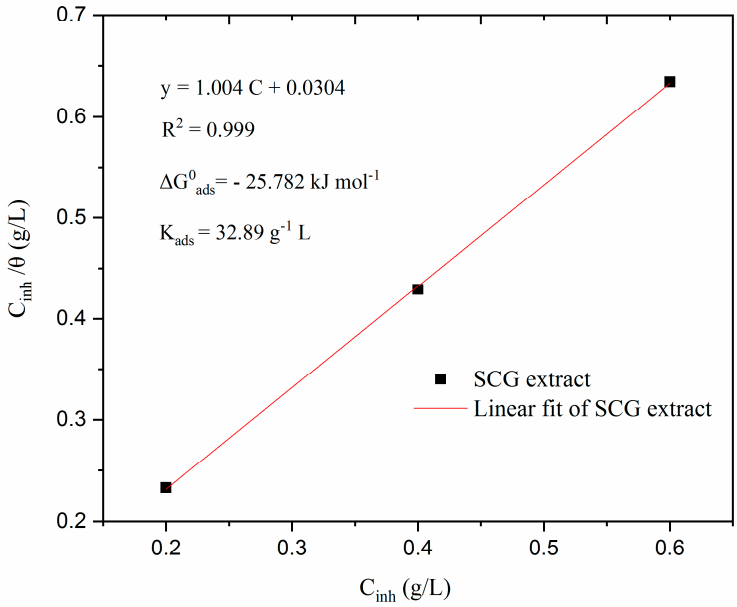

Figure 8. Langmuir adsorption isotherm plot and corresponding modeling parameters for SCG oil extract on the copper surface in 3 wt % NaCl solution at RT.

The adsorption's standard free-energy (ΔG^0_{ads}) was calculated from this isotherm through the following relation (19) [62]:

$$\Delta G^0_{ads} = RT \ln(1000\ K_{ads}) \quad (19)$$

Where R is the universal gas constant, T is the thermodynamic temperature and 1000 is the water's concentration ($g.L^{-1}$). The negative values of ΔG^0_{ads} (-25.782 $kJmol^{-1}$) refer to the spontaneity of the process and the strong interaction between the adsorption layer and the copper surface [63].

Generally, the level of the adsorption's standard free energy - around - 20 kJ mol^{-1} or less negative - can reveal that there is an electrostatic interaction between the inhibitor and the charged metal surface (physical adsorption); those around - 40 kJ mol^{-1} or less indicates a coordination between the lone pair of O atoms or π-electrons cloud and the metallic surface (chemical adsorption) [58,63]. Therefore, the calculated value of ΔG^0_{ads} is between - 40 kJ mol^{-1} and - 20 kJ mol^{-1}, indicating that the inhibitor adsorption on the copper surface occurred by a mixed process and involves both physisorption and chemisorption [25,64].

Conclusions

The current research aimed at valorizing the used coffee grounds. The physicochemical characterization (FTIR and TGA) of SCG extract proved the presence of an oily fraction. The latter was found to be an effective green inhibitor of copper in 3wt % NaCl solution. According to the potentiodynamic polarization analysis, SCG oil extract functions as a cathodic-type inhibitor by blocking the cathodic surface sites with organic compounds. The inhibition efficiency rose with the increase of the oil concentration and reached 95.78 % at a 0.6 g/L. This result is in accordance with the one obtained from EIS. An evaluation of the adsorption process proved that the SCG oil's adsorption on copper is both physical and chemical in nature and follows a Langmuir type of adsorption isotherm.

References

1. Khaled, K.F. Corrosion Control of Copper in Nitric Acid Solutions Using Some Amino Acids–A Combined Experimental and Theoretical Study. *Corrosion Science* **2010**, *52*, 3225–3234.
2. Dafali, A.; Hammouti, B.; Mokhlisse, R.; Kertit, S. Substituted Uracils as Corrosion Inhibitors for Copper in 3% NaCl Solution. *Corrosion science* **2003**, *45*, 1619–1630.
3. Hussin, M.H.; Kassim, M.J. The Corrosion Inhibition and Adsorption Behavior of Uncaria Gambir Extract on Mild Steel in 1 M HCl. *Materials Chemistry and Physics* **2011**, *125*, 461–468.
4. Kear, G.; Barker, B.D.; Walsh, F.C. Electrochemical Corrosion of Unalloyed Copper in Chloride Media—-a Critical Review. *Corrosion science* **2004**, *46*, 109–135.
5. Refait, P.; Rahal, C.; Masmoudi, M. Corrosion Inhibition of Copper in 0.5 M NaCl Solutions by Aqueous and Hydrolysis Acid Extracts of Olive Leaf. *Journal of Electroanalytical Chemistry* **2020**, *859*, 113834.
6. Nunez, L.; Reguera, E.; Corvo, F.; Gonzalez, E.; Vazquez, C. Corrosion of Copper in Seawater and Its Aerosols in a Tropical Island. *Corrosion Science* **2005**, *47*, 461–484.
7. Mellak, N.; Ghali, N.; Messaoudi, N.; Benhelima, A.; Ferhat, M.; Addou, A. Study of Corrosion Inhibition Properties of Schinus Molle Essential Oil on Carbon Steel in HCl. *Materials and Corrosion* **2021**.
8. Miralrio, A.; Espinoza Vázquez, A. Plant Extracts as Green Corrosion Inhibitors for Different Metal Surfaces and Corrosive Media: A Review. *Processes* **2020**, *8*, 942.
9. Chaubey, N.; Qurashi, A.; Chauhan, D.S.; Quraishi, M.A. Frontiers and Advances in Green and Sustainable Inhibitors for Corrosion Applications: A Critical Review. *Journal of Molecular Liquids* **2021**, *321*, 114385.
10. Alrefaee, S.H.; Rhee, K.Y.; Verma, C.; Quraishi, M.A.; Ebenso, E.E. Challenges and Advantages of Using Plant Extract as Inhibitors in Modern Corrosion Inhibition Systems: Recent Advancements. *Journal of Molecular Liquids* **2021**, *321*, 114666.
11. Wei, H.; Heidarshenas, B.; Zhou, L.; Hussain, G.; Li, Q.; Ostrikov, K.K. Green Inhibitors for Steel Corrosion in Acidic Environment: State of Art. *Materials Today Sustainability* **2020**, *10*, 100044.
12. Daoudi, W.; El Aatiaoui, A.; Dagdag, O.; Zaidi, K.; Haldhar, R.; Kim, S.-C.; Oussaid, A.; Aouinti, A.; Berisha, A.; Benhiba, F. Anti-Corrosion Coating Formation by a Biopolymeric Extract of Artemisia Herba-Alba Plant: Experimental and Theoretical Investigations. *Coatings* **2023**, *13*, 611.
13. Haldhar, R.; Vanaraj, R.; Dagdag, O.; Berisha, A.; Kim, S.-C. Convolvulus Microphyllus Extract as a Green, Effective, and Affordable Corrosion Inhibitor: Theoretical Calculations and Experimental Studies. *Coatings* **2023**, *13*, 860.
14. Ballesteros, L.F.; Teixeira, J.A.; Mussatto, S.I. Extraction of Polysaccharides by Autohydrolysis of Spent Coffee Grounds and Evaluation of Their Antioxidant Activity. *Carbohydrate polymers* **2017**, *157*, 258–266.
15. Shang, Y.-F.; Xu, J.-L.; Lee, W.-J.; Um, B.-H. Antioxidative Polyphenolics Obtained from Spent Coffee Grounds by Pressurized Liquid Extraction. *South African Journal of Botany* **2017**, *109*, 75–80.
16. Campos-Vega, R.; Loarca-Pina, G.; Vergara-Castaneda, H.A.; Oomah, B.D. Spent Coffee Grounds: A Review on Current Research and Future Prospects. *Trends in Food Science & Technology* **2015**, *45*, 24–36.
17. Gómez-de la Cruz, F.J.; Cruz-Peragón, F.; Casanova-Pelaez, P.J.; Palomar-Carnicero, J.M. A Vital Stage in the Large-Scale Production of Biofuels from Spent Coffee Grounds: The Drying Kinetics. *Fuel Processing Technology* **2015**, *130*, 188–196.
18. Karmee, S.K. A Spent Coffee Grounds Based Biorefinery for the Production of Biofuels, Biopolymers, Antioxidants and Biocomposites. *Waste management* **2018**, *72*, 240–254.

19. Bouhlal, F.; Labjar, N.; Abdoun, F.; Mazkour, A.; Serghini-Idrissi, M.; El Mahi, M.; Skalli, A.; El Hajjaji, S. Chemical and Electrochemical Studies of the Inhibition Performance of Hydro-Alcoholic Extract of Used Coffee Grounds (HECG) for the Corrosion of C38 Steel in 1M Hydrochloric Acid. *Egyptian Journal of Petroleum* **2020**, *29*, 45–52.
20. Bouhlal, F.; Labjar, N.; Abdoun, F.; Mazkour, A.; Serghini-Idrissi, M.; El Mahi, M.; Lotfi, E.M.; El Hajjaji, S. Electrochemical and Thermodynamic Investigation on Corrosion Inhibition of C38 Steel in 1M Hydrochloric Acid Using the Hydro-Alcoholic Extract of Used Coffee Grounds. *International Journal of Corrosion* **2020**, *2020*, 1–14.
21. Torres, V.V.; Amado, R.S.; De Sá, C.F.; Fernandez, T.L.; da Silva Riehl, C.A.; Torres, A.G.; D'Elia, E. Inhibitory Action of Aqueous Coffee Ground Extracts on the Corrosion of Carbon Steel in HCl Solution. *Corrosion Science* **2011**, *53*, 2385–2392.
22. Velazquez-Torres, N.; Martinez, H.; Porcayo-Calderon, J.; Vazquez-Velez, E.; Gonzalez-Rodriguez, J.G.; Martinez-Gomez, L. Use of an Amide-Type Corrosion Inhibitor Synthesized from the Coffee Bagasse Oil on the Corrosion of Cu in NaCl. *Green Chemistry Letters and Reviews* **2018**, *11*, 1–11.
23. da Costa, M.A.; Gois, J.S. de; Toaldo, I.M.; Bauerfeldt, A.C.F.; Batista, D.B.; Bordignon-Luiz, M.T.; do Lago, D.C.; Luna, A.S.; Senna, L.F. de Optimization of Espresso Spent Ground Coffee Waste Extract Preparation and the Influence of Its Chemical Composition as an Eco-Friendly Corrosion Inhibitor for Carbon Steel in Acid Medium. *Materials Research* **2020**, *23*.
24. Rahal, C.; Masmoudi, M.; Abdelhedi, R.; Sabot, R.; Jeannin, M.; Bouaziz, M.; Refait, P. Olive Leaf Extract as Natural Corrosion Inhibitor for Pure Copper in 0.5 M NaCl Solution: A Study by Voltammetry around OCP. *Journal of Electroanalytical Chemistry* **2016**, *769*, 53–61.
25. Masmoudi, F.; Jedidi, I.; Amor, Y.B.; Masmoudi, M. Corrosion Protection Evaluation of Copper Coated with a Block Copolymer and Block Coploymer/Carbon Black Nanoparticles in 3 Wt% NaCl Solution. *ChemistrySelect* **2023**, *8*, e202202608.
26. Yang, L.; Mahmood, N.; Corscadden, K.; Xu, C.C. Production of Crude Bio-Oil via Direct Liquefaction of Spent K-Cups. *Biomass and Bioenergy* **2016**, *95*, 354–363.
27. Dang, C.-H.; Nguyen, T.-D. Physicochemical Characterization of Robusta Spent Coffee Ground Oil for Biodiesel Manufacturing. *Waste and Biomass Valorization* **2019**, *10*, 2703–2712.
28. Krause, M.C.; Moitinho, A.C.; Ferreira, F.R.; Souza, R.L. de; Krause, L.C.; Caramão, E.B. Production and Characterization of the Bio-Oil Obtained by the Fast Pyrolysis of Spent Coffee Grounds of the Soluble Coffee Industry. *Journal of the Brazilian Chemical Society* **2019**, *30*, 1608–1615.
29. Lazzari, E.; Schena, T.; Marcelo, M.C.A.; Primaz, C.T.; Silva, A.N.; Ferrao, M.F.; Bjerk, T.; Caramao, E.B. Classification of Biomass through Their Pyrolytic Bio-Oil Composition Using FTIR and PCA Analysis. *Industrial Crops and Products* **2018**, *111*, 856–864.
30. Lyman, D.J.; Benck, R.; Dell, S.; Merle, S.; Murray-Wijelath, J. FTIR-ATR Analysis of Brewed Coffee: Effect of Roasting Conditions. *Journal of agricultural and food chemistry* **2003**, *51*, 3268–3272.
31. Wang, J.; Jun, S.; Bittenbender, H.C.; Gautz, L.; Li, Q.X. Fourier Transform Infrared Spectroscopy for Kona Coffee Authentication. *Journal of food science* **2009**, *74*, C385–C391.
32. Raba, D.N.; Poiana, M.-A.; Borozan, A.B.; Stef, M.; Radu, F.; Popa, M.-V. Investigation on Crude and High-Temperature Heated Coffee Oil by ATR-FTIR Spectroscopy along with Antioxidant and Antimicrobial Properties. *PloS one* **2015**, *10*, e0138080.
33. Phimsen, S.; Kiatkittipong, W.; Yamada, H.; Tagawa, T.; Kiatkittipong, K.; Laosiripojana, N.; Assabumrungrat, S. Oil Extracted from Spent Coffee Grounds for Bio-Hydrotreated Diesel Production. *Energy Conversion and Management* **2016**, *126*, 1028–1036.
34. Atabani, A.E.; Shobana, S.; Mohammed, M.N.; Uğuz, G.; Kumar, G.; Arvindnarayan, S.; Aslam, M.; Al-Muhtaseb, A.H. Integrated Valorization of Waste Cooking Oil and Spent Coffee Grounds for Biodiesel Production: Blending with Higher Alcohols, FT–IR, TGA, DSC and NMR Characterizations. *Fuel* **2019**, *244*, 419–430, doi:10.1016/j.fuel.2019.01.169.
35. Vlachos, N.; Skopelitis, Y.; Psaroudaki, M.; Konstantinidou, V.; Chatzilazarou, A.; Tegou, E. Applications of Fourier Transform-Infrared Spectroscopy to Edible Oils. *Analytica chimica acta* **2006**, *573*, 459–465.
36. Jović, O.; Smolić, T.; Jurišić, Z.; Meić, Z.; Hrenar, T. Chemometric Analysis of Croatian Extra Virgin Olive Oils from Central Dalmatia Region. *Croatica Chemica Acta* **2013**, *86*, 335–344.
37. Lyman, D.J.; Benck, R.; Dell, S.; Merle, S.; Murray-Wijelath, J. FTIR-ATR Analysis of Brewed Coffee: Effect of Roasting Conditions. *J. Agric. Food Chem.* **2003**, *51*, 3268–3272, doi:10.1021/jf0209793.

38. Moharam, M.A.; Abbas, L.M. A Study on the Effect of Microwave Heating on the Properties of Edible Oils Using FTIR Spectroscopy. *African Journal of Microbiology Research* **2010**, *4*, 1921–1927.
39. Ballesteros, L.F.; Teixeira, J.A.; Mussatto, S.I. Chemical, Functional, and Structural Properties of Spent Coffee Grounds and Coffee Silverskin. *Food and bioprocess technology* **2014**, *7*, 3493–3503.
40. Todaka, M.; Kowhakul, W.; Masamoto, H.; Shigematsu, M. Thermal Analysis and Dust Explosion Characteristics of Spent Coffee Grounds and Jatropha. *Journal of Loss Prevention in the Process Industries* **2016**, *44*, 538–543, doi:10.1016/j.jlp.2016.08.008.
41. Dhouibi, I.; Masmoudi, F.; Bouaziz, M.; Masmoudi, M. A Study of the Anti-Corrosive Effects of Essential Oils of Rosemary and Myrtle for Copper Corrosion in Chloride Media. *Arabian Journal of Chemistry* **2021**, *14*, 102961.
42. Masmoudi, M.; Abdelmouleh, M.; Abdelhedi, R. Infrared Characterization and Electrochemical Study of γ-Methacryloxypropyltrimethoxysilane Grafted in to Surface of Copper. *Spectrochimica Acta Part A: Molecular and Biomolecular Spectroscopy* **2014**, *118*, 643–650.
43. Rahal, C.; Masmoudi, M.; Abdelmouleh, M.; Abdelhedi, R. An Environmentally Friendly Film Formed on Copper: Characterization and Corrosion Protection. *Progress in Organic Coatings* **2015**, *78*, 90–95.
44. Elmorsi, M.A.; Hassanein, A.M. Corrosion Inhibition of Copper by Heterocyclic Compounds. *Corrosion science* **1999**, *41*, 2337–2352.
45. Raza, M.A.; Rehman, Z.U.; Ghauri, F.A. Corrosion Study of Silane-Functionalized Graphene Oxide Coatings on Copper. *Thin Solid Films* **2018**, *663*, 93–99.
46. Yu, Y.; Yang, D.; Zhang, D.; Wang, Y.; Gao, L. Anti-Corrosion Film Formed on HAl77-2 Copper Alloy Surface by Aliphatic Polyamine in 3 Wt.% NaCl Solution. *Applied Surface Science* **2017**, *392*, 768–776.
47. Nam, N.D.; Ha, P.T.N.; Anh, H.T.; Hoai, N.T.; Hien, P.V. Role of Hydroxyl Group in Cerium Hydroxycinnamate on Corrosion Inhibition of Mild Steel in 0.6 M NaCl Solution. *Journal of Saudi Chemical Society* **2019**, *23*, 30–42.
48. Sui, W.; Zhao, W.; Zhang, X.; Peng, S.; Zeng, Z.; Xue, Q. Comparative Anti-Corrosion Properties of Alkylthiols SAMs and Mercapto Functional Silica Sol–Gel Coatings on Copper Surface in Sodium Chloride Solution. *Journal of Sol-Gel Science and Technology* **2016**, *80*, 567–578.
49. Bouhlal, F.; Mazkour, A.; Labjar, H.; Benmessaoud, M.; Serghini-Idrissi, M.; El Mahi, M.; El Hajjaji, S.; Labjar, N. Combination Effect of Hydro-Alcoholic Extract of Spent Coffee Grounds (HECG) and Potassium Iodide (KI) on the C38 Steel Corrosion Inhibition in 1M HCl Medium: Experimental Design by Response Surface Methodology. *Chemical Data Collections* **2020**, *29*, 100499.
50. Hassairi, H.; Bousselmi, L.; Khosrof, S.; Triki, E. Evaluation of the Inhibitive Effect of Benzotriazole on Archeological Bronze in Acidic Medium. *Applied Physics A* **2013**, *113*, 923–931.
51. Hong, S.; Chen, W.; Zhang, Y.; Luo, H.Q.; Li, M.; Li, N.B. Investigation of the Inhibition Effect of Trithiocyanuric Acid on Corrosion of Copper in 3.0 Wt.% NaCl. *Corrosion Science* **2013**, *66*, 308–314.
52. Qiang, Y.; Zhang, S.; Xu, S.; Li, W. Experimental and Theoretical Studies on the Corrosion Inhibition of Copper by Two Indazole Derivatives in 3.0% NaCl Solution. *Journal of colloid and interface science* **2016**, *472*, 52–59.
53. Ghelichkhah, Z.; Sharifi-Asl, S.; Farhadi, K.; Banisaied, S.; Ahmadi, S.; Macdonald, D.D. L-Cysteine/Polydopamine Nanoparticle-Coatings for Copper Corrosion Protection. *Corrosion Science* **2015**, *91*, 129–139.
54. Li, Z.; Wang, X.; Zhang, Y.; Jing, C. Enhancing the Corrosion Resistance of Epoxy Coatings by Impregnation with a Reduced Graphene Oxide-Hydrophobic Ionic Liquid Composite. *ChemElectroChem* **2018**, *5*, 3300–3306.
55. Peng, S.; Zeng, Z.; Zhao, W.; Li, H.; Xue, Q.; Wu, X. Synergistic Effect of Thiourea in Epoxy Functionalized Silica Sol–Gel Coating for Copper Protection. *Surface and Coatings Technology* **2012**, *213*, 175–182.
56. Dueke-Eze, C.U.; Madueke, N.A.; Iroha, N.B.; Maduelosi, N.J.; Nnanna, L.A.; Anadebe, V.C.; Chokor, A.A. Adsorption and Inhibition Study of N-(5-Methoxy-2-Hydroxybenzylidene) Isonicotinohydrazide Schiff Base on Copper Corrosion in 3.5% NaCl. *Egyptian Journal of Petroleum* **2022**, *31*, 31–37.
57. Bentiss, F.; Lebrini, M.; Lagrenée, M. Thermodynamic Characterization of Metal Dissolution and Inhibitor Adsorption Processes in Mild Steel/2, 5-Bis (n-Thienyl)-1, 3, 4-Thiadiazoles/Hydrochloric Acid System. *Corrosion science* **2005**, *47*, 2915–2931.

 doi:10.20944/preprints202306.0568.v1

58. Pourriahi, M.; Nasr-Esfahani, M.; Motalebi, A. Effect of Henna and Rosemary Extracts on the Corrosion of 304L Stainless Steel in 3.5% NaCl Solution. *Surface Engineering and Applied Electrochemistry* **2014**, *50*, 525–533.
59. Fateh, A.; Aliofkhazraei, M.; Rezvanian, A.R. Review of Corrosive Environments for Copper and Its Corrosion Inhibitors. *Arabian journal of Chemistry* **2020**, *13*, 481–544.
60. Ramos, S.A.F.; Senna, L.F. de; Lago, D.C.B. do Evaluation of Aqueous Coffee Husks Extracts as a Corrosion Inhibitor of 1020 Carbon Steel in 1 Mol L-1 HCl Solution. *Materials Research* **2019**, *22*.
61. Deyab, M.A. Corrosion Inhibition of Aluminum in Biodiesel by Ethanol Extracts of Rosemary Leaves. *Journal of the Taiwan Institute of chemical Engineers* **2016**, *58*, 536–541.
62. Zhang, H.H.; Qin, C.K.; Chen, Y.; Zhang, Z. Inhibition Behaviour of Mild Steel by Three New Benzaldehyde Thiosemicarbazone Derivatives in 0.5 M H2SO4: Experimental and Computational Study. *Royal Society open science* **2019**, *6*, 190192.
63. Masmoudi, M.; Rahal, C.; Abdelhedi, R.; Khitouni, M.; Bouaziz, M. Inhibitive Action of Stored Olive Mill Wastewater (OMW) on the Corrosion of Copper in a NaCl Solution. *RSC advances* **2015**, *5*, 101768–101775.
64. de Souza, F.S.; Giacomelli, C.; Gonçalves, R.S.; Spinelli, A. Adsorption Behavior of Caffeine as a Green Corrosion Inhibitor for Copper. *Materials Science and Engineering: C* **2012**, *32*, 2436–2444.